To appear in: *Cement and Concrete Composites*

(Special issue with papers from ICDC 2012)

June 2013

Updating of service-life prediction of reinforced concrete structures with potential mapping

Sylvia Keßler[1*], Johannes Fischer[2], Daniel Straub[2], Christoph Gehlen[1]

[1]Centre for Building Materials, Technische Universität München, Germany
[2]Engineering Risk Analysis Group, Technische Universität München, Germany

*Corresponding author: E-mail address: kessler@cbm.bv.tum.de (Sylvia Keßler)

Abstract

Fully probabilistic models are available for predicting the service life of new reinforced concrete structures and for condition assessment of existing structures. Frequently, the decisive mechanism limiting the service life of reinforced concrete structures is chloride-induced corrosion, for which these models predict probabilistically the time to corrosion initiation. Once the corrosion process is initiated, corroding areas can be detected nondestructively through potential mapping. The spatial information gained from potential mapping can then be used for updating the service-life prediction, taking into consideration the spatial variability of the corrosion process. This paper introduces the spatial updating of the probabilistic model with potential mapping and concrete cover measurements by means of Bayesian analysis. A case study is presented, where potential mapping is applied prior to a destructive assessment, which serves to verify the approach. It is found that the potential mapping can provide significant information on the condition state. With the presented methods, this information can be consistently included in the probabilistic service-life prediction.

Keywords: Life cycle prediction; potential mapping; updating; spatial variability.

1 Introduction

The fib Model Code for Service Life Design [1] provides methods for a fully probabilistic service-life prediction for reinforced concrete (RC) structures subject to corrosion of the reinforcement. For chloride-induced corrosion of the reinforcement, such methods facilitate the probabilistic prediction of the time to corrosion initiation. The model code, however, does not address the spatial variability of the occurrence of corrosion. Degradation of reinforced concrete structures varies in space due to variation of geometry (e. g. concrete cover), concrete properties, (e. g. chloride-migration), and exposure conditions (e. g. chloride impact). Local inaccuracies of the construction process lead to additional spatial variability of corrosion. When planning maintenance and repair activities, it is essential that this spatial variability is considered. In the literature, several studies (Hergenröder [2], Faber et. al. [3], Malioka [4]) perform spatial modeling of the corrosion initiation phase such as chloride ingress and carbonation through a subdivision of the structure into elements. The element size is determined by the spatial variability of the most important parameter of the corrosion initiation model. The spatial variability of the corrosion propagation phase is considered e. g. in Li et al. [5], and Stewart and Mullard [6].

Additional information on the beginning and extent of corrosion can be obtained through condition assessments, e. g. by means of visual inspection and non-destructive testing such as potential-field measurement. The inspection data not only provide information on the temporal development of corrosion, but also enable an improved spatial description of corrosion. It is possible to combine the results from these condition assessments with the probabilistic models of corrosion through Bayesian updating. Using the data gained from inspection, Bayesian updating is possible for single model parameters, for the deterioration model itself, and for the deterioration probability. The incorporation of inspection data into the corrosion model by means of Bayesian updating has demonstrated in the past [3,7-9]. A computationally efficient method for updating the reliability with measurement data is proposed in [10].

This paper presents a procedure for Bayesian updating of the corrosion probability using combined spatial data from both cover-depth and potential-field measurement on an existing RC slab subject to chloride-induced corrosion of the reinforcement. The procedure is applied to a case study, and the updated probabilistic predictions are compared to the actual conditions as identified during the replacement of the concrete cover.

2 Methodology

2.1 Service-life prediction

The presentation hereafter is limited to chloride-induced corrosion of the reinforcement. In concrete, embedded reinforcement is protected against corrosion due to the high alkalinity of the pore solution. A thin iron oxide layer, the so called passive layer, is formed. The passive layer can be destroyed locally by ingress of chlorides coming from deicing salt or seawater if a critical chloride concentration is exceeded at the steel surface. This initiation period, i.e. the probability of depassivation, can be calculated with a fully probabilistic model [1, 11]. The corrosion process is initiated as soon as the concentration of chloride ions (equation (1)) exceeds a certain critical concentration C_{crit} at the level d_c of the reinforcement.

A diffusion model is applied to estimate the chloride concentration at the level d_c of the reinforcement. With given surface concentration C_S and diffusion coefficient D, the concentration of chloride ions at time t in depth d_c is given by

$$C(d_c, t) = C_S \cdot \left(1 - \mathrm{erf}\left(\frac{d_c}{2\sqrt{D\ t}}\right)\right). \quad (1)$$

In this equation, D is assumed to be constant. However, this is not the case in reality [1,11]. To adapt the diffusion model to the actual environmental onsite conditions, to specific concrete properties, and to account for its time-dependency, the diffusion coefficient D in equation (2) is modified following [1,11] to

$$D(t) = D_{RCM,0} \cdot k_e \cdot k_t \cdot \left(\frac{t_0}{t}\right)^a. \quad (2)$$

The chloride-ingress model is based on a solution of Fick's second law of diffusion assuming that diffusion is the dominant transport mechanism. However, Fick's diffusion law is not suitable for describing the transport mechanisms in the near-surface layer, since it assumes a stationary surface concentration of chloride ions in time. In reality, due to intermittent wetting and drying, the surface concentration and varies with time. For that reason, the diffusion is modeled only beyond the depth of a convection layer Δz, where a substitute surface concentration of $C_{S,\Delta z}$ is applied. Modifying equation (1) accordingly and inserting the time-dependent diffusion coefficient of equation (2), one obtains

$$C(d_c, t) = C_{S,\Delta z} \cdot \left(1 - \mathrm{erf}\left(\frac{d_c - \Delta z}{2\sqrt{D_{RCM,0}\ k_e\ k_t \cdot \left(\frac{t_0}{t}\right)^a \cdot t}}\right)\right) \quad (3)$$

with the deterioration model parameters:

C_{crit}	Critical corrosion inducing chloride content at depth of reinforcement [wt.-%/cem.],
$C_{S,\Delta z}$	Substitute surface chloride concentration at depth Δz [wt.-%/cem.],
d_c	Concrete cover depth [mm],
Δz	Thickness of the convection zone layer [mm],
$D_{RCM,0}$	Rapid chloride migration coefficient [mm²/a],
k_e	Factor for considering temperature impact on $D_{RCM,0}$ [-],
k_t	Transfer parameter (test method) [-],
t_0	Reference testing time ($t_0 = 28$ d) [a],
a	Aging exponent [-].

The dimensionless correction factor k_e accounts for the influence of the actual onsite temperature and is given by

$$k_e = \exp\left(b_e \cdot \left(\frac{1}{T_{ref}} - \frac{1}{T_{real}}\right)\right), \quad (4)$$

where T_{real} is the onsite temperature, T_{ref} is the reference temperature, and b_e is a regression parameter (all in [K]) [1,11].

Finally, the event of corrosion at time t is written as

$$F_t = \left\{ C_{\text{crit}} - C_{\text{S},\Delta z} \cdot \left(1 - \text{erf}\left(\frac{d_c - \Delta z}{2\sqrt{D_{\text{RCM},0}\, k_{\text{e}}\, k_{\text{t}} \cdot \left(\frac{t_0}{t}\right)^{a} \cdot t}} \right) \right) \leq 0 \right\} \tag{5}$$

Most of the parameters in equation (5) are modeled as random variables. In the case study presented later, specific probability distribution models for these parameters are presented.

Let now $\mathbf{X} = \left[C_{\text{crit}}, C_{\text{S},\Delta z}, d_c, \Delta z, D_{\text{RCM},0}, k_{\text{e}}, k_{\text{t}}, a\right]^{\text{T}}$ be the vector of the model's basic random variables with their joint PDF $f_{\mathbf{X}}(\mathbf{x})$, and Ω_{F_t} denotes the domain in the outcome space of $\mathbf{X}$ corresponding to the event F_t . The corrosion probability is then given by

$$\Pr(F_t) = \int_{\Omega_{F_t}} f_{\mathbf{X}}(\mathbf{x})\ \mathrm{d}x_1\, \mathrm{d}x_2 \ldots \mathrm{d}x_n \tag{6}$$

wherein $\int_{\Omega_{F_t}} \mathrm{d}x_1 \ldots \mathrm{d}x_n$ denotes the integration over the failure domain Ω_{F_t}. This integral can be evaluated using any structural reliability method (SRM), such as FORM or Monte-Carlo methods [12,13].

2.1.1 Random field modeling of corrosion

Some of the model parameters vary randomly in space. As an example, consider the concrete cover depth at a certain location A. With high probability, the cover depth at a neighboring location will have a value similar to the one in A, whereas the cover depth at a faraway location is likely to be independent of the one in A. To account for such spatial correlation of model parameters, they are modeled as spatial random fields. Random field modeling of corrosion in RC structures has been presented in several studies; e.g. [3,14,15]. Using a second-order description of the random field, it is necessary to specify the spatial covariance matrix in addition to the marginal probability distributions.

In the case study presented later, all spatially varying parameters are described by homogenous, isotropic random fields. The spatial covariance matrix of any random variable X is described by a monotonically decreasing function:

$$[\mathbf{C}_{XX}]_{i,j} = \text{Cov}\left[X_i, X_j\right] = \sigma_X^2 \exp\left(-\frac{dist_{ij}}{l_X}\right), \tag{7}$$

with

$dist_{ij}$ Distance between location i and j [m],
l_X Correlation length of the random variable X [m],
σ_X Standard deviation of the random variable X [Unit of the variable itself].

2.2 Updating the service-life prediction

2.2.1 Bayesian updating

When measurement data from inspection or monitoring are available, these can be directly used for updating the probability of corrosion. The model updating after an inspection is straightforward by applying Bayes' rule:

$$\Pr(\text{Condition}|\text{Inspection}) = c \times \Pr(\text{Inspection}|\text{Condition})\,\Pr(\text{Condition}), \tag{8}$$

where c is a normalizing constant ensuring that the sum or the integral over all possible conditions results in one. $\Pr(\text{Condition})$ represents the prior knowledge on the structural condition coming from the a-priori service-life prediction. $\Pr(\text{Inspection}|\text{Condition})$ is the likelihood of the observed inspection result for a given condition. Finally, $\Pr(\text{Condition}|\text{Inspection})$ is the a-posteriori probability of a specific condition given the inspection result. A detailed description of the implementation of the Bayesian updating procedure is presented in [10,14,15].

For updating, three different types of measurements are potentially available: The first type are measurements of a direct model parameter of the deterioration model; in the case study, we use onsite measured data of the cover depth d_c. The second type includes direct or indirect measurements of the condition state; in the case study we use measurement data from potential mapping. The third type is given by measuring quantities that are related to the condition state through the deterioration model, e. g. measurements of the chloride concentration at certain depths (see e.g. [14, 15]). The updating with the measurements available in the case study is described in the following two sections.

2.2.2 Updating with data from cover depth measurement

Since the cover depth d_c is a direct model parameter in equation (5), we may update the corrosion probability by updating only the probability density function (PDF) of the cover depth, $f_{d_c}(d_c)$, and then use the posterior PDF $f''_{d_c}(d_c)$ in the probabilistic calculation. Since the cover depth is modeled as a discretized random field, the updating must be performed on the joint PDF of the cover depth at all n discrete locations on the surface.

Using the measurement data $\mathbf{d}_{\text{m}} = [d_{\text{m}1}, d_{\text{m}2}, \dots, d_{\text{m}n}]^{\text{T}}$, the mean value $\mathbf{m}_{d_c}$ and the covariance matrix $\mathbf{C}_{d_c d_c}$ (introduced in equation (7)) of the cover depth are updated following the procedure described in [14]. The posterior corrosion probability is estimated using (6), by replacing $f_{d_c}(d_c)$ with its posterior $f''_{d_c}(d_c)$.

2.2.3 Updating with data from potential mapping

An effective inspection method is the potential mapping, which is able to indicate corroding (active) and noncorroding (passive) areas in RC structures [16]. Therefore, potential mapping data is used to check if and where corrosion has started. Potential mapping yields information about the corrosion condition state at the time of the measurement; direct statements about corrosion processes in the past or future are not possible. The advantage of potential mapping is that measurements can be performed in a grid over the whole structure or a component, and, in this way, potential mapping delivers spatial information on the corrosion condition state.

During potential mapping, the potential difference U_{m} between an external reference electrode and the reinforcement is measured. A lower potential indicates a higher probability of corrosion. Exemplarily, Figure 1 shows the potential differences measured on the RC element considered in the case study. The data is summarized in a histogram of 50 equally spaced intervals of width 10 mV.

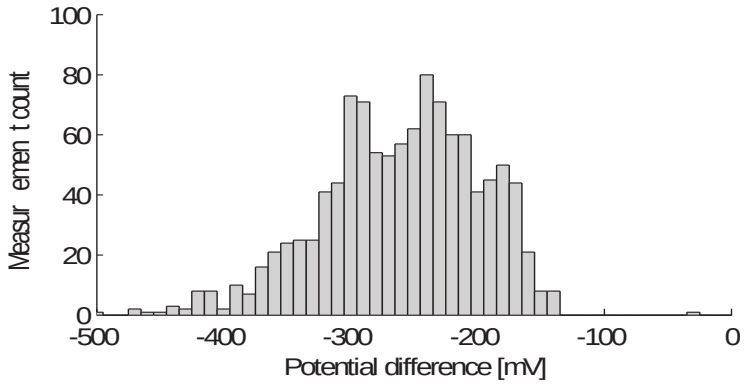

Figure 1: The histogram of the measured potential differences.

To perform the probability updating with the potential mapping U_{m}, the domains where the reinforcement is either active or passive should be distinguished. Since it is not possible to deterministically identify a threshold potential, a probabilistic approach is pursued as described in the following.

Commonly, the potential differences in the active and the passive areas are modeled as normally distributed [17]. Using the Maximum Likelihood Estimate (MLE) method for parameter estimation [18,19], it is possible to find the two normal distributions that fit the data most suitable. This is illustrated in Figure 2: The black curve denotes the PDF of the potential difference given the reinforcement is active, F, and the black dashed curve shows the PDF of the potential difference given the reinforcement is passive, $\bar{F}$. The gray curve represents the combined PDF of the potential differences, $f_U(u)$.

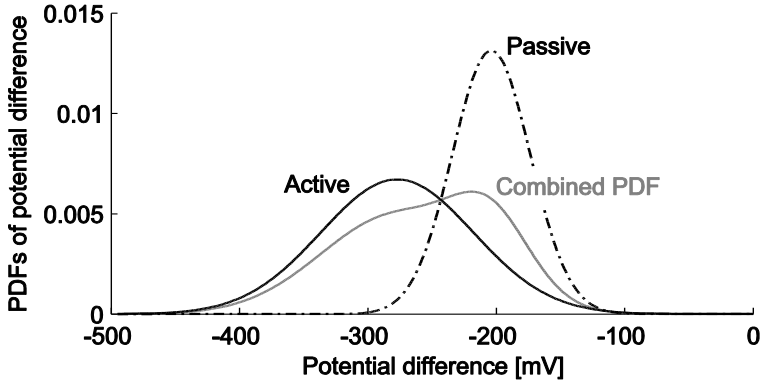

Figure 2: The density functions of the potential difference for active (black) and passive (black dashed) reinforcement, as well as their combined PDF (gray).

In Figure 3, the cumulative density function (CDF) of the fitted combined distribution is compared to the empirical CDF, which corresponds to the histogram of Figure 1. The figure indicates a good fit between potential measurement and the combined distribution estimated by MLE.

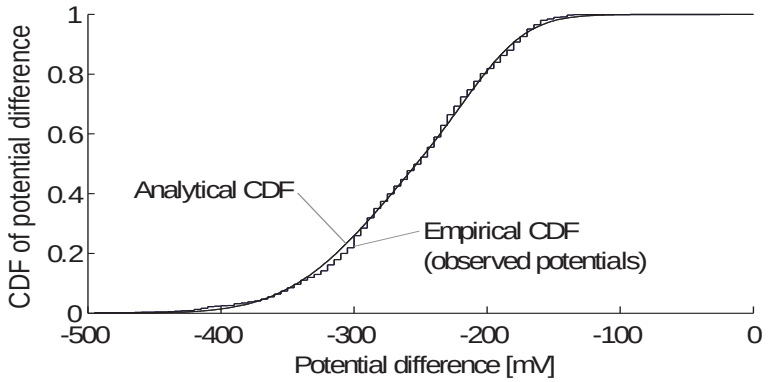

Figure 3: The analytical CDF of the measured potential differences $\mathbf{u}_{\mathrm{m}}$ estimated by MLE agrees with the empirical CDF.

From Figure 2 it can be observed that - for the examined structure - potentials lower than -300 mV are likely to be associated with corroding reinforcement. For potential values larger than -300 mV, the corrosion probability decreases with increasing potentials. As can be recognized in Figure 2, there is a large domain where the active and the passive distribution overlap. In this domain, the likelihood of planning the wrong measures is higher: either a repair is executed although it is not necessary, or a wrong all-clear may result in further damage and additional costs in the future.

To calculate the updated depassivation probability, $\Pr(F_i|u_{\mathrm{m}})$, the rule for conditional probabilities depicted in equation (8) is applied for each element i on the concrete surface. Using the density function for the active corrosion, $f_{U|F}(u_i|F)$, as estimated earlier, the probability updating becomes

$$\Pr(F_i|u_{\mathrm{m}}) = \frac{f_{U|F}(u_i|F)\cdot \Pr(F)}{f_{U|F}(u_i|F)\cdot \Pr(F) + f_{U|\bar{F}}(u_i|\bar{F})\cdot \Pr(\bar{F})}\ . \tag{9}$$

3 Numerical investigation

3.1 Case study

The case study is a reinforced concrete underpass in a city with increasing traffic volume, shown in Figure 4. Due to the climate and the traffic situation, the structure belongs to the exposure class XD3 following EN 206-1 [20], which is characterized by cyclic wetting and drying in combination with severe chloride impact. The underpass was built in 1961. The inspection data were generated in 2008 when the structure was 47 years old. The underpass consists of abutments and retaining walls. Each side of the underpass is longer than 200 m. For a better overview, only the evaluation of one section of the retaining wall is presented (field 14, as indicated in Figure 4).

Figure 4: Underpass with the selected section of the retaining wall: field 14 (marked) [Source: GoogleEarth].

3.2 Probabilistic model

Due to the age of the structure, information on the concrete composition and properties is not available. Considering the materials and codes commonly used during time of construction, it is assumed that a Portland cement with a water/binder ratio of 0.5 was used. The probabilistic service-life prediction is calculated using the input parameters of Table 1, which were obtained for the specific material and environmental conditions from [1]. For the spatial modeling, the correlation length of all spatially varying parameters is assumed to be $l_X = 2.0\,\text{m}$.

The prior corrosion probability computed with Monte-Carlo simulation (MCS) is shown in Figure 5. The calculation is based on data of Table 1. Since no spatial information is available a-priori, the corrosion probability is equal for each element on the whole surface. At the time of the inspection, in year 47, the probability of corrosion initiation is 60 %.

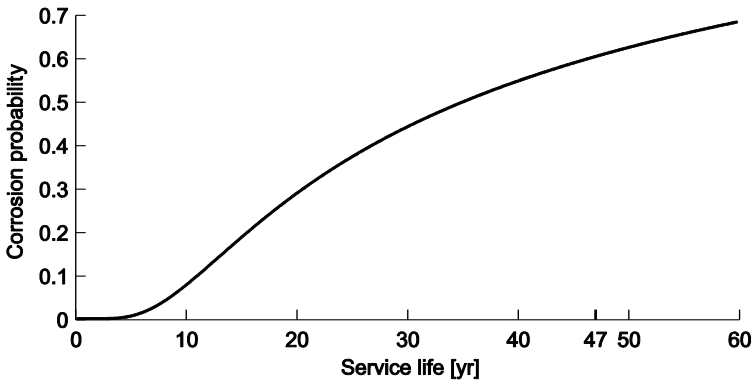

Figure 5: Prior corrosion probability of the reinforcement calculated with MCS.

Table 1: The random model input parameters, their distributions, and distribution parameters for the full probabilistic corrosion initiation model following the fib bulletin [1], further data from [11].

Parameter X_k		**Unit**	**Distribution**	μ_{X_k}	σ_{X_k}	l_{X_k}
$D_{\text{RCM},0}$		[10^{-12} m²/s]	Normal	498.3	99.7	2.0
a		[-]	Beta $0 \leq a \leq 1$	0.3	0.12	∞
t_0		[a]	-	0.0767		∞
t_{insp}		[a]	-	47		∞
k_{t}		[-]	-	1	-	-
	T_{ref}	[K]	-	293		-
k_{e}	T_{real}	[K]	Normal	282	3	-
	b_{e}	[K]	Normal	4800	700	-
$C_{\text{s},\Delta z}$		[wt.%/cem.]	Lognormal	2.73	1.23	2.0
C_{crit}		[wt.%/cem.]	Beta $0 \leq C_{\text{crit}} \leq 2$	0.6	0.15	∞
Δz		[mm]	Beta $0 \leq \Delta z \leq 50$	8.9	5.6	2.0
d_c		[mm]	Lognormal	40	13	2.0

3.3 Inspection data

Concrete cover measurements and potential mapping were performed on the entire surface. The measurement grid was chosen as $0.25\,\text{m} \times 0.5\,\text{m}$ in x and y direction, respectively. The following illustrations in Figure 6 show the inspection data obtained from field 14. The histogram of measured potential differences is given in Figure 1.

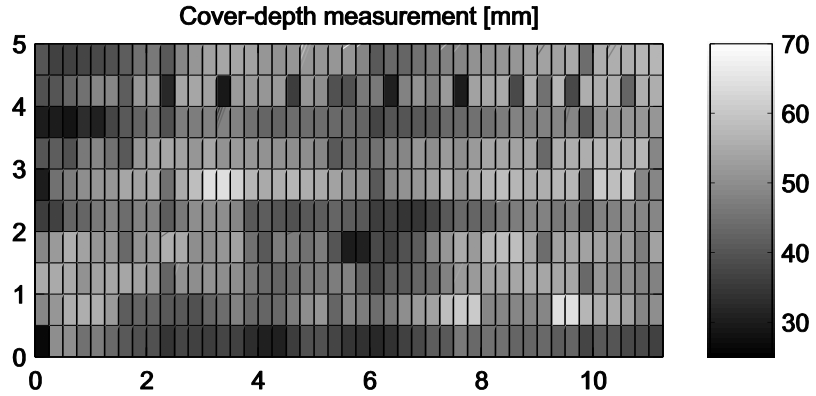

(a) Results from cover depth measurement over the whole surface in [mm].

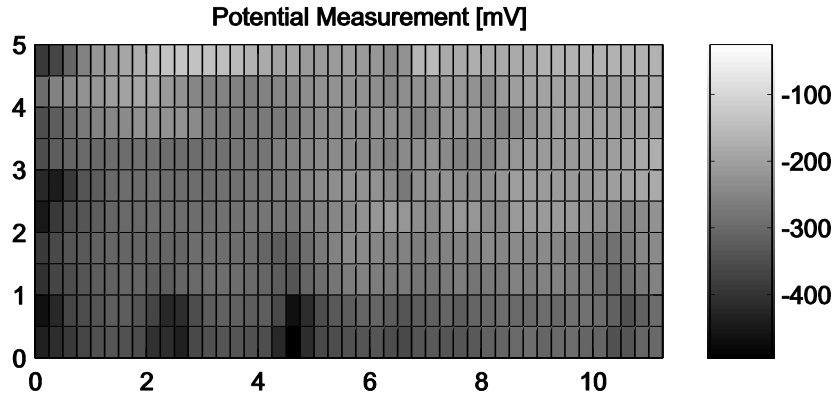

(b) Results from potential mapping over the whole surface in [mV].

Figure 6: Inspection data from field 14: **(a)** concrete cover measurement; **(b)** potential mapping.

The spatial variability of the concrete cover can be observed from the measurement results in Figure 6a. The measured concrete cover d_{m} varies in the range of 25 mm and 55 mm, which corresponds well to the a-priori model with mean value of $\mu_{d_c} = 40$ mm and standard deviation $\sigma_{d_c} = 13$ mm.

The potential mapping data (Figure 1 and Figure 6b) shows measured potential differences in the range of -450 mV to -100 mV. Visually, one can already observe areas with low potentials and, therefore, higher likelihood of corrosion on the left side and at the bottom.

3.4 Updating the service-life prediction with inspection data

The corrosion probability is updated spatially using the methods described in section 2.2 for the time of inspection $t_{\mathrm{insp}} = 47$ yr. Figure 7 and Figure 8 show the probability of corrosion updated with each inspection method - concrete cover measurement and potential mapping - individually. Finally, Figure 9 shows the probability of corrosion updated with the results of both measurements.

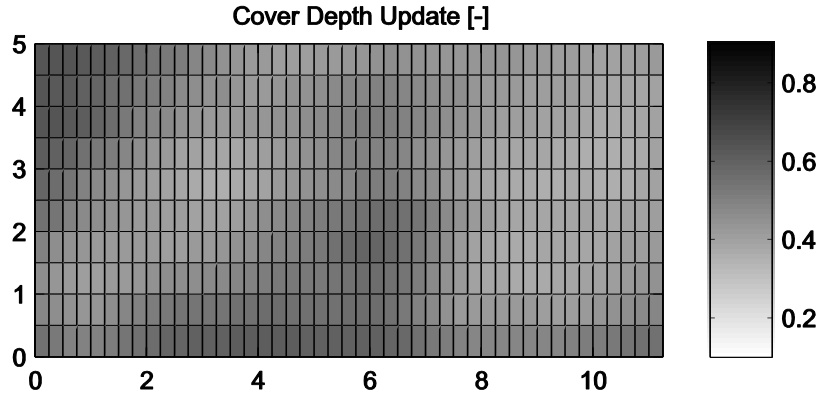

Figure 7: Updated corrosion probability on the scale from 0.1 to 0.9 over the whole surface of field 14 using data from cover depth measurement.

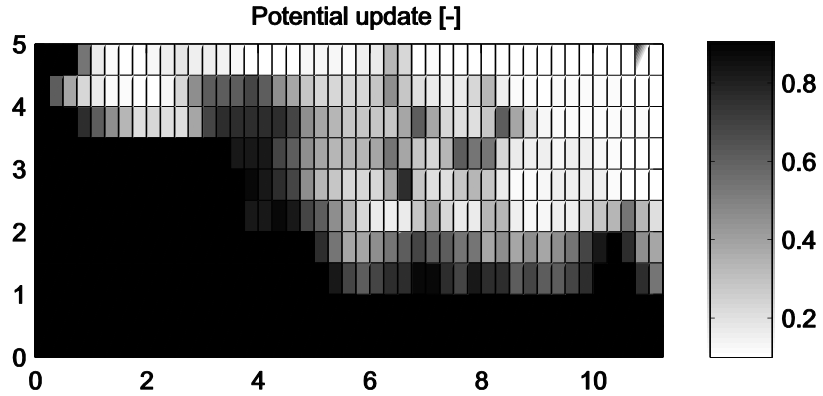

Figure 8: Updated corrosion probability over the whole surface of field 14 using potential mapping data.

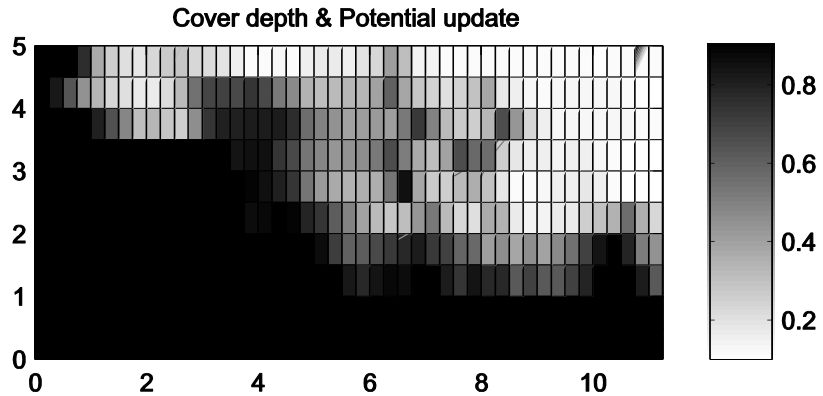

Figure 9: Updated corrosion probability over the whole surface of field 14 using data from both cover depth measurement and potential mapping.

The model updated with cover depth measurements (Figure 7) shows corrosion probabilities between 20 % and 60 %. Major parts of the area have a corrosion probability of 20 %. Two spots with higher corrosion probabilities are in the left side above and in the middle below.

The corrosion probability after updating with potential mapping data (Figure 8) indicates a division of the inspected field diagonal into two parts. The left side and the lower parts have high corrosion probabilities with values of over 90 %. Along the boundary to the top right side, corrosion probabilities of approximately 60 % down to 0 % are calculated.

The updating with potential mapping and the updating with cover depth give different results. The concrete cover measurements cannot directly predict the deterioration condition and its interpretation depends on the model. In particular, the model does not take into account the actual spatial distribution of the chloride impact and singularities in the structure, such as the joint on the left side of field 14, where chloride-contaminated water from the road above could flow off. With advanced age of the structure, potential mapping indirectly reflects the spatial distribution of the chloride impact. This is the case above, where the zone with chloride-contaminated water is clearly identifiable.

The combined updating of the corrosion probability using data from both cover depth measurement and potential mapping (Figure 9) indicates similar results as the update using only potential mapping data. In the case of a structure with significant active corrosion, the potential mapping appears to provide more information than the more indirect cover depth measurement.

It is noted that the corrosion probability is high in general. This is explained partly by the fact that the structure is relatively old and exposed to one of the most aggressive exposure conditions, as already reflected in the prior probability.

3.5 Comparison of the updated corrosion probabilities to the real condition

Following the inspection results, the structure was repaired. The outer concrete cover was replaced until behind the first reinforcement layer. Therefore, the corrosion condition of the reinforcement was visible in the form of loss of cross section. Figure 10 shows the loss of cross section map.

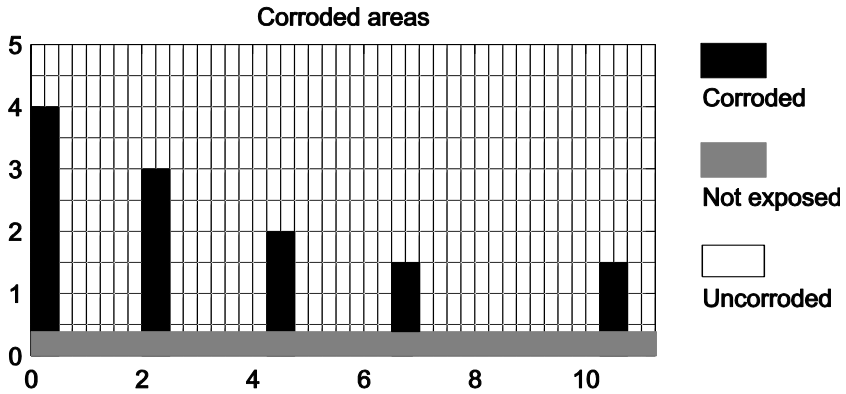

Figure 10: Loss of cross section (marked) identified through visual inspection.

The observed corrosion condition ranges from superficial corrosion with a roughened surface to complete loss of cross section. With visual inspection, one cannot indicate all corroding areas, because the reinforcement exhibits no loss of cross section where corrosion has just started.

Comparing the updated corrosion probability (Figure 9) to the real condition (Figure 10), a larger corroding area was predicted than revealed by the visual inspection.

This result can be explained in two ways. Firstly, as stated above, visual inspection is not able to identify all corroding areas. Secondly, an electrochemical effect takes place that is not accounted for in the model: The reinforcement surface around a corroding area automatically behaves as a cathode. So this surrounding area is thus naturally protected against corrosion. The expansion of the resulting potential field due to an anode can reach more than one meter [21]. Consequently, low potentials are measured at the concrete surface, although the

reinforcement under the concrete surface is a cathode. This explains the non-corroding areas in-between the corroding ones.

The corrosion-probability updating has identified all corroding areas; no anode area was overlooked. However, also some non-corroding areas were indicated as corroding. Therefore, the updating criterion for the potential mapping data appears to be conservative. Additional research is needed to identify a more differentiated criterion for updating the service life prediction with potential mapping.

4 Summary and outlook

Maintaining the serviceability of aging reinforced concrete structures is a major task in infrastructure management. Probabilistic service-life prediction with additional consideration of inspection data is a powerful tool to support this task. This paper presents a case study of an updating of the service-life prediction of a concrete structure with concrete-cover measurements and potential-mapping data. The special innovation of this procedure is the consideration of the spatial variability of the deterioration process. Inspection and maintenance planning can be executed more precisely by taking into account the spatial variability of the deterioration process. As a result, this approach enables the reduction of maintenance costs over the life cycle of structures.

The presented case study indicates that the potential mapping provides more information on the corrosion probability for structures in which corrosion has already initiated. Concrete-cover measurements exhibit the advantage of being time-independent. Therefore, they can be applied already at an early stage before corrosion starts. As shown by the visual inspection of the reinforcement, the computed posterior probabilities correspond well to the actual corrosion state of the structure.

The next step to complete the presented framework is the implementation of the corrosion propagation model, which will enable the prediction of the probability of cross section loss of the steel reinforcement, and therefore allows predicting the reliability of concrete structures.

Acknowledgment

The authors wish to thank the engineering consultancy Ingenieurbüro Schießl Gehlen Sodeikat GmbH and the Munich administration for supporting the project by providing the measurement data.

5 References

1. Schießl P, Bamforth P, Baroghel-Bouny, V, Corley G, Faber M, Forbes J, Gehlen C, et al. Model code for service life design. fib bulletin 34, 2006

2. Hergenröder M. (1992). Zur Statistischen Instandhaltungsplanung für bestehende Bauwerke bei Karbonatisierung des Betons und möglicher Korrosion der Bewehrung. Berichte aus dem Konstruktiven Ingenieurbau 4/92, TU München. (German)

3. Faber MH, Straub D, Maes MA. A Computational Framework for Risk Assessment of RC Structures Using Indicators, Computer-Aided Civil and Infrastructure Engineering 21, 2006 216-230.

4. Malioka V. Condition Indicators for the Assessment of Local and Spatial Deterioration of Concrete Structures, Diss ETH No. 18333, 2009.

5. Li Y, Vrouwenvelder T, Wijnants GH, Walraven J (2004). Spatial variability of concrete deterioration and repair strategies. Structural Concrete, 5(3): 121–129.

6. Stewart MG, Mullard JA (2007). Spatial time-dependent reliability analysis of corrosion damage and the timing of first repair for RC structures, Engineering Structures, 29(7), 1457–1464.

7. Maes MA (2002). Updating performance and reliability of concrete structures using discrete empirical Bayes methods. Journal of Offshore Mechanics and Arctic Engineering, ASME, 124(4): 239–246.

8. Straub D., Malioka V., Faber M.H. (2009). A framework for the asset integrity management of large deteriorating concrete structures. *Structure and Infrastructure Engineering*, **5**(3) pp. 199 - 213.

9. Schoefs F, Tran TV, Bastidas-Arteaga E. Optimization of inspection and monitoring of structures in case of spatial fields of deterioration properties, Proceeding ICASP, Zürich 2011

10. Straub D. Reliability updating with equality information. Probabilistic Engineering Mechanics, 26(2), 254-258, 2011

11. Gehlen C. Probabilistische Lebensdauerbemessung von Stahlbetonbauwerken: Zuverlässigkeitsbetrachtungen zur wirksamen Vermeidung von Bewehrungskorrosion. Berlin: Beuth, 2000 (Deutscher Ausschuss für Stahlbeton 510). – ISBN 978-3-410-65710-1, 2000 (German).

12. Ditlevsen O. Uncertainty modeling with applications to multidimensional civil engineering systems. New York McGraw-Hill, 1981. – ISBN 0-07-017046-0

13. Ditlevsen O, Madsen HO. Structural reliability methods. Chichester: Wiley, 1996. – ISBN 0 471 96086 1

14. Fischer J, Straub D. Reliability Assessment of Corroding Reinforced Concrete Slabs with inspection Data. In: 9th Int. Probabilistic Workshop Braunschweig, 2011

15. Straub D. Spatial reliability assessment of deteriorating reinforced concrete surfaces with inspection data. Proc. ICASP 2011, Zürich, 2011

16. Menzel K, Preusker H. Potentialmessung: Eine Methode zur zerstörungsfreien Feststellung von Korrosion an der Bewehrung. Bauingenieur 64, 181-186, 1989 (German)

17. Elsener B, Böhni H. Electrochemical methods for the inspection of reinforcement corrosion. Concrete structures-field experience. Material Science Forum, 1992:635-646.

18. Lindley DV. Introduction to Probability & Statistics. Cambridge University Press, 1965

19. Benjamin JR, Cornell CA. Probability, Statistics and Decision for Civil Engineers. McGraw-Hill Book Company, New York, USA, 1970.

20. EN 206-1/ DIN 1045-2

21. Keßler S, Gehlen C. Potential mapping - Possibilities and limits. In: 8th fib PhD Symposium 20-23 June 2010 in Lyngby, Denmark.